


Particle and vapor emissions from vat polymerization desktop-scale 3-dimensional printers

A. B. Stefaniak, L. N. Bowers, A. K. Knepp, T. P. Luxton, D. M. Peloquin, E. J. Baumann, J. E. Ham, J. R. Wells, A. R. Johnson, R. F. LeBouf, F.-C. Su, S. B. Martin & M. A. Virji


To cite this article: A. B. Stefaniak, L. N. Bowers, A. K. Knepp, T. P. Luxton, D. M. Peloquin, E. J. Baumann, J. E. Ham, J. R. Wells, A. R. Johnson, R. F. LeBouf, F.-C. Su, S. B. Martin & M. A. Virji (2019) Particle and vapor emissions from vat polymerization desktop-scale 3-dimensional printers, Journal of Occupational and Environmental Hygiene, 16:8, 519-531, DOI: [10.1080/15459624.2019.1612068](https://doi.org/10.1080/15459624.2019.1612068)

To link to this article: <https://doi.org/10.1080/15459624.2019.1612068>

 View supplementary material 

 Published online: 16 May 2019.




 Submit your article to this journal 

 Article views: 103

 View Crossmark data 



Particle and vapor emissions from vat polymerization desktop-scale 3-dimensional printers

A. B. Stefaniak^a , L. N. Bowers^a, A. K. Knepp^a, T. P. Luxton^b , D. M. Peloquin^c , E. J. Baumann^d, J. E. Ham^a, J. R. Wells^a, A. R. Johnson^a, R. F. LeBouf^a, F.-C. Su^a, S. B. Martin, Jr.^a, and M. A. Virji^a

^aNational Institute for Occupational Safety and Health, Morgantown, West Virginia; ^bU.S. Environmental Protection Agency, Office of Research and Development, National Risk Management Research Laboratory, Cincinnati, Ohio; ^cOak Ridge Institute for Science and Education, Oak Ridge, Tennessee; ^dPegasus Technical Services, Cincinnati, Ohio

ABSTRACT

Little is known about emissions and exposure potential from vat polymerization additive manufacturing, a process that uses light-activated polymerization of a resin to build an object. Five vat polymerization printers (three stereolithography (SLA) and two digital light processing (DLP) were evaluated individually in a 12.85 m³ chamber. Aerosols (number, size) and total volatile organic compounds (TVOC) were measured using real-time monitors. Carbonyl vapors and particulate matter were collected for offline analysis using impingers and filters, respectively. During printing, particle emission yields (#/g printed) ranged from 1.3 ± 0.3 to $2.8 \pm 2.6 \times 10^8$ (SLA printers) and from 3.3 ± 1.5 to $9.2 \pm 3.0 \times 10^8$ (DLP printers). Yields for number of particles with sizes 5.6 to 560 nm (#/g printed) were 0.8 ± 0.1 to $2.1 \pm 0.9 \times 10^{10}$ and from 1.1 ± 0.3 to $4.0 \pm 1.2 \times 10^{10}$ for SLA and DLP printers, respectively. TVOC yield values ($\mu\text{g/g}$ printed) ranged from 161 ± 47 to 322 ± 229 (SLA printers) and from 1281 ± 313 to 1931 ± 234 (DLP printers). Geometric mean mobility particle sizes were 41.1–45.1 nm for SLA printers and 15.3–28.8 nm for DLP printers. Mean particle and TVOC yields were statistically significantly higher and mean particle sizes were significantly smaller for DLP printers compared with SLA printers ($p < 0.05$). Energy dispersive X-ray analysis of individual particles qualitatively identified potential occupational carcinogens (chromium, nickel) as well as reactive metals implicated in generation of reactive oxygen species (iron, zinc). Lung deposition modeling indicates that about 15–37% of emitted particles would deposit in the pulmonary region (alveoli). Benzaldehyde (1.0–2.3 ppb) and acetone (0.7–18.0 ppb) were quantified in emissions from four of the printers and 4-oxopentanal (0.07 ppb) was detectable in the emissions from one printer. Vat polymerization printers emitted nanoscale particles that contained potential carcinogens, sensitizers, and reactive metals as well as carbonyl compound vapors. Differences in emissions between SLA and DLP printers indicate that the underlying technology is an important factor when considering exposure reduction strategies such as engineering controls.

KEYWORDS



3-dimensional printing; digital light processing; stereolithography; ultrafine particles; vat polymerization; volatile organic compounds

Introduction

With additive manufacturing (AM) technologies developing and expanding rapidly across the world, health scientists are struggling to keep up with exposure research. Gaps remain in knowledge about emissions and exposure potential from various types of AM, including vat polymerization. Although AM has been used in industrial settings for several decades, the recent commercial availability of smaller,

inexpensive desktop printers, so-called “3-D printers,” has greatly expanded their use to non-industrial spaces, such as schools, libraries, and private homes. This expansion, and the fact that several types of AM processes release potentially hazardous particles and/or vapors,^[1–12] necessitates an evaluation of the full vat polymerization processes to understand emissions.

Vat polymerization is a type of AM process in which a liquid photopolymer resin in a vat is selectively cured by light-activated polymerization to build

CONTACT A. B. Stefaniak  ASTefaniak@cdc.gov  National Institute for Occupational Safety and Health, 1095 Willowdale Road, Morgantown, West Virginia 26505.

Color versions of one or more of the figures in the article can be found online at www.tandfonline.com/uoeh.

 Supplemental data for this article can be accessed at tandfonline.com/uoeh. AIHA and ACGIH members may also access supplementary material at <http://oeh.tandfonline.com>.

This work was authored as part of the Contributor's official duties as an Employee of the United States Government and is therefore a work of the United States Government. In accordance with 17 U.S.C. 105, no copyright protection is available for such works under U.S. Law.

an object.^[13] Vat polymerization differs from other types of AM processes such as material extrusion, material jetting, binder jetting, and powder bed fusion in that building an object involves hardening a bulk liquid, rather than extruding melted filament, depositing liquid droplets, adhering powder together, or binding powder, respectively. The main components of the photopolymer resins used in vat polymerization machines are binders (50–80%), monomers (10–40%), and photoinitiators (<10%).^[14] Binders are long-chain molecules that impart shape and mechanical properties to an object, and include molecules such as acrylates and epoxies,^[14] which are known immune sensitizers.^[15–17] Monomers are added to reduce the viscosity of the photopolymer.^[14] Photoinitiators are light sensitive molecules that react with the binders and monomers to make long-chain molecules that cross-link and harden.^[14] A number of light sensitive, and potentially toxic, materials are used as photoinitiators, including antimony oxide, copper, zinc, and iron complexes, and titanium, aluminum, and barium compounds.^[14,18–21]

Emerging reports suggest there is potential for adverse health effects from exposures incurred during operation of some AM machines. For example, exposure to emissions from material extrusion 3-D printers using acrylonitrile butadiene styrene (ABS) filaments have been attributed to a case of work-related asthma and development of acute hypertension in experimental animals.^[22,23] In a survey of additive manufacturing workers, 59% reported suffering from respiratory symptoms, including (but not limited to) nasal congestion, rhinorrhea, cough, and itchy nose, throat, or eyes, at least once per week.^[24]

Understanding emissions from vat polymerization AM processes is critical because these desktop 3-D printers are used in a wide variety of settings, the feedstock resin contains immune sensitizers and toxic metals, and other types of AM technology have already proven to be detrimental to respiratory and cardiovascular health. The purposes of this study were to measure particle and total volatile organic compound concentrations and calculate emission rates for different types of desktop-scale vat polymerization AM printers to better understand exposure potential.

Materials and methods

3-D printers and feedstock materials

Table 1 summarizes the five desktop vat polymerization printers evaluated in this study. Types of vat polymerization technology include, but are not limited

Table 1. Vat polymerization printers and gray resins evaluated in chamber tests.

Model	Manufacturer	Type	Resin Brand
Form 1+	Formlabs	SLA	Formlabs
Pegasus Touch	Full Spectrum Laser	SLA	Alchemy Universal
Nobel 1.0A	XYZPrinting	SLA	XYZPrinting
Titan 1	Kudo3-D	DLP	Spot – HT Hard and Tough
M-One	MakeX	DLP	Formlabs

SLA = stereolithography, DLP = digital light processing

to, stereolithography (SLA) and digital light processing (DLP). SLA printers scan a laser beam across the print area to selectively cure resin in a vat. This process cures the resin as series of points and rounded lines to build objects layer-by-layer. DLP printers use a high-resolution projector to flash black and white image slices of each object layer across the entire vat surface at once. The projector is a digital screen that forms white areas of the projected image made of square pixels that are cured using multi-wavelength light from a lamp to build an object. In this study, three were SLA type and two were DLP type. All printers used gray liquid feedstock resins. Elemental content from photoinitiators in the bulk feedstock resins and pieces of printed objects was determined by microwave assisted acid extraction following EPA Method 3051A, and subsequent analysis by inductively coupled plasma mass spectroscopy (ICP-MS). Briefly, 0.1 g of bulk resin or shavings from a printed object was placed into a pre-cleaned 50 mL Teflon digestion vessel along with 9 mL of trace metal grade nitric acid and 3 mL of trace metal grade hydrochloric acid. The vessels were capped and placed in a microwave (MARS 6 Xpress, CEM, Matthews, NC). The samples were heated to 175 °C and extracted for 10 min at pressure. Samples were cooled and diluted to a final volume of 50 mL. A single sample of bulk liquid resin was digested whereas triplicate samples obtained from different locations of a printed object were digested to account for potential spatial variability. Elemental analysis was conducted on an ICP-MS (Agilent 7900, Agilent Technologies, Santa Clara, CA). Sample analyses were conducted in both no gas and collision mode using helium (5.0 mL/min).

To characterize the properties of particles in the feedstock, resin was drop-cast onto 3- μ m pore size track-etched polycarbonate (TEPC) filters, allowed to air dry, and analyzed using a field emission scanning electron microscope (FE-SEM, S-4800, Hitachi, Tokyo, Japan) to determine particle morphology and energy dispersive X-ray analysis (EDX, Quantax, Bruker Scientific Instruments, Berlin, Germany) to identify

elemental constituents. Additionally, pieces of printed objects were mounted on aluminum sample stubs using double-sided carbon tape and evaluated using FE-SEM-EDX.

Test chamber

All printing was performed in a temperature ($21 \pm 1^\circ\text{C}$) and humidity ($50 \pm 5\%$) controlled 12.85 m^3 stainless steel chamber meeting international guidelines for emissions testing.^[25] Using SF_6 , the calculated mixing level (η) was 92% (a level above 80% is considered satisfactory), the leak rate was 0.024 air changes per hour, and the air exchange rate was 1 per hour.^[26] Air entering the chamber was passed through a carbon filter and high efficiency particulate air (HEPA) filter to remove organic vapors and particles, respectively.

Chamber air was sampled for at least 30 min prior to printing to establish background using the real-time instrumentation and time-integrated sampling approaches for particles and organic chemicals (described below). All print jobs were of an artifact from the National Institute of Standards and Technology (NIST).^[27] The artifact has a $10\text{ cm} \times 10\text{ cm}$ square base and is 1 cm thick with various features to test printer performance, including fine features (depressions, holes, and protruding pins) as well as larger features (holes, protruding pins, elevated staircases and a ramp). The same artifact was printed five times per printer at 50% scale of full size ($5\text{ cm} \times 5\text{ cm} \times 1\text{ cm}$). Print times ranged from 78–192 min, depending on the machine.

Air sampling

Real-time instruments and time-integrated sampling approaches were used to measure particle and volatile organic chemical levels in the chamber (Figure S1 in the Supplemental File). Separate samples were collected during the background phase and printing phase (including the decay period, which lasted for three chamber air exchanges after completion of printing).

Total particle number concentration from 20 nm to $1\text{ }\mu\text{m}$ (Model 8525, P-Trak, TSI Inc., Shoreview, MN) and size distribution of particles from 5.6–560 nm (Model 3091, fast mobility particle sizer [FMPS], TSI Inc.) were measured inside the chamber. The P-trak counts ultrafine and sub-micron particles by sampling air at 0.1 L/min (0.7 L/min total flow). As particles are aspirated into the instrument, they are passed through

a saturated isopropyl alcohol vapor, which condenses on the particles and grows their size large enough to scatter laser light and be detected by the instrument. Particle counts were logged at a 10-sec interval. The FMPS samples air at 10 L/min. As particle-laden air is aspirated into the instrument, the particles are positively charged using a corona charger. The charged particles are detected using multiple electrometers and enumerated based on their mobility size in 32 size channels. Particle counts and sizes were logged at a 1-sec interval. Airborne particles were collected on TEPC filters during printing by drawing chamber air through filters at up to 10 L/min using a calibrated sampling pump (SG10-2, GSA Messgerätebau GmbH, Ratingen, Germany). All filters were analyzed using FE-SEM-EDX.

Total volatile organic compound (TVOC) concentration was monitored using a real-time photoionization detector (PID) (RAE Systems, San Jose, CA or Ion Science Inc., Stafford, TX) with a 10.6 eV lamp. This instrument uses an ultraviolet light to ionize organic molecules (with an ionization potential below 10.6 eV); the positively charged ions are detected as changes in electrical current by the instrument. Measurements were logged on a 1-sec basis. The potential for chemical emissions from the printers to react with ozone to form secondary chemical compounds such as carbonyl compounds was evaluated by drawing air through liquid impingers at 4 L/min for three of the five trials per printer, followed by derivatization and analysis using GC-MS.^[28]

Calculation of emission rates and yields

Particle emission rates (ER) were calculated from the real-time measurement data collected during printing using a mass-balance model.^[8] From the real-time particle concentration data logged by the P-Trak or FMPS, the ER was calculated using Equation (1):

$$ER(t) = \frac{V}{\Delta t} [C(t + \Delta t) - C(t) + R \cdot C(\text{mean}) \cdot \Delta t], \quad (1)$$

where t = time, sec.

Δt = time difference between two successive data points, sec;

$C(t + \Delta t)$ = particle number concentration at $(t + \Delta t)$, particles/ cm^3 ;

$C(t)$ = particle number concentration at (t) , particles/ cm^3 ;

V = chamber volume, cm^3 ;

R = air exchange rate in the chamber, hr^{-1}

Table 2. Average emission yields and particle sizes during printing for five vat polymerization printers (n = 5).

Printer	Type	#/g printed ^A	# 5.6 to 560 nm/g printed ^A	GM, nm (GSD) ^B	μg TVOC/g printed ^A
Form 1+	SLA	$2.7 \pm 1.6 \times 10^8$	$1.3 \pm 0.2 \times 10^{10}$	41.3 (1.7)	277.1 ± 81.5
Pegasus Touch	SLA	$1.3 \pm 0.3 \times 10^8$	$7.6 \pm 0.9 \times 10^9$	41.1 (1.8)	160.7 ± 47.4
Nobel 1.0A	SLA	$2.8 \pm 2.6 \times 10^8$	$2.1 \pm 0.9 \times 10^{10}$	45.1 (1.6)	321.7 ± 228.7
Titan 1	DLP	$9.2 \pm 3.0 \times 10^8$	$4.0 \pm 1.2 \times 10^{10}$	15.3 (1.4)	1280.5 ± 313.3
M-One	DLP	$3.3 \pm 1.5 \times 10^8$	$1.1 \pm 0.3 \times 10^{10}$	28.8 (1.5)	1931.2 ± 234.4

^AValues are arithmetic mean ± standard deviation^BValues are geometric mean (GM) and geometric standard deviation (GSD)

$C(\text{mean})$ = mean particle concentration between (t) and (t + Δt), particles/cm³.

Emission rates for TVOCs were calculated in accordance with RAL-UZ-205.^[29] ER values were calculated from the beginning of the print phase (from start to end of print job) until one air exchange occurred in the post-operating phase using Equation (2):

$$ER = \frac{c_s \cdot n_d^2 \cdot v_c \cdot t_g \cdot SER_B \cdot n_d \cdot t_g}{n_d \cdot t_d - e^{-n_d(t_g - t_d)} + e^{-n_d \cdot t_g}}, \quad (2)$$

where c_s = concentration during printing and post-decay phases, n_d = air exchange rate (h⁻¹) during printing and post-decay phases, v_c = chamber volume (m³), t_g = total sampling time (h), SER_B = specific emission rate during background phase (μg/h), and t_d = printing time (h).

To account for differences in print time among printers, the ER values were converted to total particle number or TVOC mass and normalized to the mass of resin used to build an object (determined gravimetrically using a calibrated microbalance) to calculate yield (emission per unit mass printed).^[4]

Statistical analysis

Temporal changes in particle size distributions (including median and variance) from real-time FMPS measurements were estimated using a two-level Bayesian model with a Markov chain Monte Carlo algorithm developed by Klein Entink et al.^[30] We used 1-min averages of FMPS real-time measurements for two emission tests as examples. A run of the Pegasus Touch SLA printer had 315 one-minute average measurements, of which, the 1st to 35th 1-min average measurements were background, 36th to 191st were collected during the printing phase, and the 192nd to 315th were the post-printing phase. A run of the M-One DLP printer had 214 measurements, of which, the 1st to 42nd, 43rd to 147th, and 148th to 214th 1-min average measurements were collected during the background, printing, and post-printing phases, respectively. Analyses were conducted in R 3.3.1 using the “NanoPSDA” package (R Foundation for Statistical Computing, Vienna, Austria).^[31,32]

Mean yield and particle size distribution values were compared using one-way Analysis of Variance (ANOVA) models. Specific pairwise differences between printers or types (SLA or DLP) were compared using Tukey's tests. A significance level of $\alpha = 0.05$ was used for all comparisons. Statistics were computed using JMP software (version 13, SAS Institute Inc., Cary, NC).

The fraction of emitted particles that could deposit in the lung were calculated using the Multiple-Path Particle Dosimetry model (MPPD, v3.04, ARA).^[33] Dosimetry estimates were made using the stochastic morphometric lung model with 60th percentile size to represent the majority of the general human population. This model uses morphometric measurements of the tracheobronchial tree (length, diameter, branching angle, cross-sectional area, etc.) supplemented with theoretical reconstructions of the alveolar region to predict particle deposition via the primary mechanisms of impaction, sedimentation, and diffusion. Model parameters were as follows: uniformly expanding flow, upright body position, oronasal-mouth breather with 0.5 inspiratory fraction and no pause fraction. International Commission for Radiological Protection (ICRP) reference human default values breathing parameters for a Caucasian adult male at light level of activity were used: functional residual capacity (3,300 mL), upper respiratory tract volume of 50 mL, tidal volume (1,000 mL), and breath frequency (20/min).^[34]

Results

Aerosol emissions

Table 2 summarizes the average particle emission yield values for each printer (individual yield values and size distribution measurements for each trial for each printer are provided in the Supplemental File, Tables S1–S4). ANOVA analysis indicated a significant difference in mean particle number yield values (P-Trak data) among printers ($p < 0.05$). Pairwise comparison revealed that the yield for the Titan 1 was significantly higher than all other printers ($p < 0.05$). The mean particle emission yield was higher for DLP type printers compared to SLA type printers ($p < 0.05$).

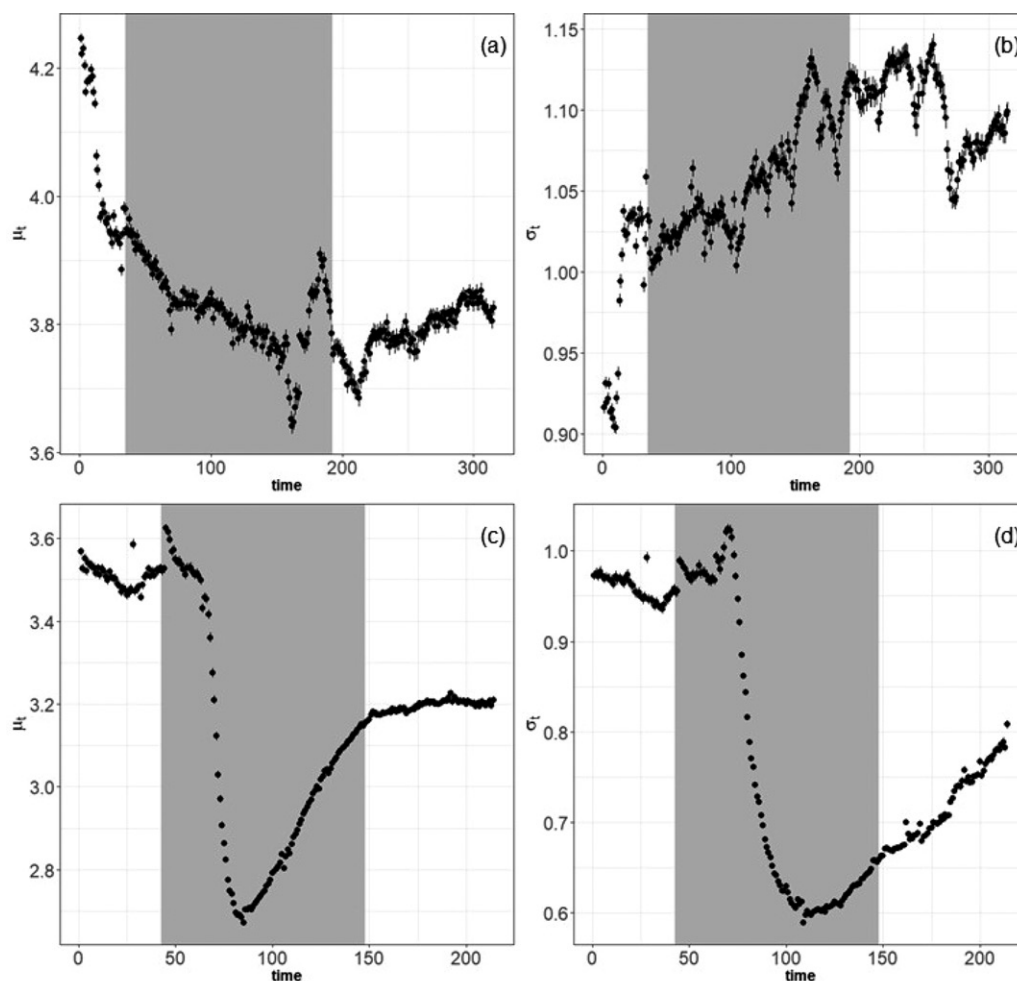


Figure 1. Time series plots (in minutes) of: panels (a) and (c) the mean (μ_t) and panels (b) and (d) standard deviation (σ_t) of two 3-D printer emission tests. Panels (a) and (b) are results for the Pegasus SLA printer, and panels (c) and (d) are results for the M-One DLP printer. The gray area indicates the printing period. Black dots are mean values with Bayesian 95% credible intervals. All y-axes are log-scale.

We used all FMPS size channels (5.6–560 nm) to calculate yield values (see Table 2). ANOVA analysis indicated a significant difference in mean number yield among printers ($p < 0.05$). Pairwise comparison revealed that the yield for the Titan 1 printer was greater than for all other printers and that the yield for the Nobel 1.0A printer was significantly higher than for the Pegasus Touch printer ($p < 0.05$). The mean yield for particles with sizes 5.6–560 nm was significantly higher for DLP-type printers compared to SLA type printers ($p < 0.05$).

Table 2 also includes the average geometric mean (GM) and geometric standard deviation (GSD) of particle sizes measured using the FMPS during printing. There were no statistical differences in the average GM mobility diameter for the Form 1+ (41.3 nm), Pegasus Touch (41.1 nm), and Nobel 1.0A (45.1 nm) printers. The average GM diameter of particles emitted by the M-One printer (28.8 nm) was significantly

larger than the Titan 1 printer (15.3 nm); ($p < 0.05$). The mean mobility size for DLP-type printers (22.0 nm) was significantly smaller than the mean size for the SLA printers (42.5 nm) ($p < 0.05$).

The results of model-fitted particle size distributions using real-time measurements are shown in Figure 1. This logarithmic regression model revealed that particle size changes among the background, printing, and post-printing phases. For the Pegasus Touch printer example, the estimated GM of the particle size distributions decreased from $\exp(4.04) = 56.8$ nm in the background period to $\exp(3.82) = 45.6$ nm in the printing period, and then to $\exp(3.79) = 44.3$ nm in the post-print decay period (Figure 1a). However, the standard deviation gets larger over these three time phases (Figure 1b). For the M-One printer example, the estimated GM particle size distributions also decreased from the background period (33.4 nm) to the printing period (21.3 nm), but slightly rebounded in the decay

Table 3. Identities of elements in bulk feedstock resin, airborne particles emitted during vat polymerization 3-D printing, and printed objects.

Printer	Resin	Elemental composition ^{A,B}		
		Bulk feedstock resin by ICP	Airborne particles by EDX	Printed objects by ICP
Form 1+	Form Labs	Al, Cr, P, Sb, Sn, Ti	<i>Ca, Cr, Fe, Ni, Si</i>	<i>Al, As, Ca, Cd, Co, Cr, Cu, Fe, Mo, Mn, Ni, P, Pb, Sb, Sn, Ti, V, Zn</i>
M-One	Form Labs	Al, Cr, P, Sb, Sn, Ti	<i>Al, Cl, Fe, Na, P, Si, Ti</i>	<i>Al, As, Ca, Cd, Co, Cr, Cu, Fe, Mo, Mn, Ni, P, Pb, Sb, Sn, Ti, V, Zn</i>
Pegasus Touch	Alchemy Universal	Al, Ba, Cr, P, Sb, Sn, Ti	<i>Al, Ca, Fe, Na, S, Si</i>	<i>Al, As, Ba, Ca, Cd, Co, Cr, Cu, Fe, Mo, Mn, Ni, P, Pb, Sb, Sn, Ti, V, Zn</i>
Noble 1.0A	XYZPrinting	Al, Cr, P, Sn, Ti	<i>Al, Cr, Fe, Mg, Ni, P, Si, Zn</i>	<i>Al, As, Ca, Cd, Co, Cr, Cu, Fe, Mo, Mn, Ni, P, Pb, Sb, Sn, Ti, V, Zn</i>
Titan 1	Spot – HT	Al, Cr, Cu, P, Pb, Sn, Ti	<i>Al, Ba, Fe, Mg, Na, P, S, Si, Zn</i>	<i>Al, As, Ca, Cd, Co, Cr, Cu, Fe, Mo, Mn, Ni, P, Pb, Sb, Sn, Ti, V, Zn</i>

^AICP = inductively coupled plasma-mass spectrometry, EDX = energy dispersive X-ray analysis. Al = aluminum, As = arsenic, Ba = barium, Ca = calcium, Cd = cadmium, Cl = chlorine, Co = cobalt, Cr = chromium, Cu = copper, Fe = iron, Mg = magnesium, Mn = manganese, Mo = molybdenum, Na = sodium, Ni = nickel, P = phosphorous, Pb = lead, S = sulfur, Sb = antimony, Si = silicon, Sn = tin, Ti = titanium, V = vanadium, Zn = zinc

^BElements in bold font are present in both the bulk resin and airborne particles, elements in italics are present in both the airborne particles and the built object.

period (24.3 nm) (Figure 1c). The standard deviation decreased over these three time phases (Figure 1d).

Inorganic elemental composition of resins, emitted particles, and built objects

Analysis of bulk resins, emitted particles, and built objects indicates that vat polymerization chemistry is highly complex. Table 3 summarizes the identities of elements present throughout the vat polymerization AM process. Nine different elements were identified in the bulk feedstock resins, 14 different elements were identified in the airborne particles, and 19 elements of health interest were found amongst the printed object samples.

Supplemental Table S5 summarizes the ICP-MS measurements for concentrations of elements in the bulk feedstock resins. Aluminum (Al), chromium (Cr), phosphorous (P), tin (Sn), and titanium (Ti) were detected in all resins, though concentrations varied among brands. Antimony (Sb), Ba, copper (Cu), and lead (Pb) were quantifiable in some but not all of the bulk resins. In addition to ICP analysis of the liquid resin, samples of dried resin were inspected using FE-SEM-EDX. Analysis identified discrete particles and cluster particles (Supplemental Figure S2) that were composed of single and/or multiple elements (Supplemental Figure S3).

Figure 2 shows the morphology and Figure 3 shows the corresponding elemental composition of exemplar airborne particles emitted during operation of the vat polymerization printers. Regardless of the resin brand or printer type all filter samples contained branch chain aggregates of nanoscale spherical primary particles which, from EDX analysis, were composed of carbon and oxygen (Figures 2a and 3a). In addition to these branch chain particles, each printer emitted submicron-scale compact particles with variable elemental composition (Figures 2b–2f, 3b–3f). Only iron (Fe) was identified in

the aerosol emissions from all of the printers. Particles emitted by the Form 1+ printer included single-constituent calcium (Ca), Si, and Fe particles, multi-constituent particles containing Fe and nickel (Ni), and particles containing Fe, Ni, and Cr. The M-One printer emitted single-constituent particles that contained Fe, Si, Ti, or P as well as multi-constituent particles. Particles emitted by the Pegasus Touch printer included single-constituent Al particles as well as multi-constituent particles containing Ca, Fe, sodium (Na), sulfur (S), and/or Si. During operation of the Nobel 1.0A printer, multi-constituent particles were emitted that included Cr, Ni, and zinc (Zn). For the Titan 1 printer, emitted particles included Fe or Si particles as well as multi-constituent particles, some of which contained Ba.

Supplemental Table S5 summarizes the ICP-MS measurements for concentrations of elements in the printed objects. ICP analysis of printed objects identified the same elements as in the bulk feedstock resins, as well as several additional metals: arsenic (As), cadmium (Cd), Ca, cobalt (Co), Fe, manganese (Mn), molybdenum (Mo), Ni, vanadium (V), and Zn. With the exception of Sb and P, elements were more concentrated in the printed objects than in the corresponding bulk resins. Table 3 shows that ICP analysis identified a total of 19 different elements in the printed objects; all but Ba were common among samples. Although Formlabs resin was used in both the M-One and Form 1+ printers, concentrations of five elements (Cd, Cr, Co, Ni, and V) were higher in objects printed with the M-One compared with the Form 1+ printer.

Aerosol lung deposition estimates

Table 4 summarizes the regional deposition fractions for the respiratory tract for particles emitted by each type of vat polymerization printer. Deposition fractions were

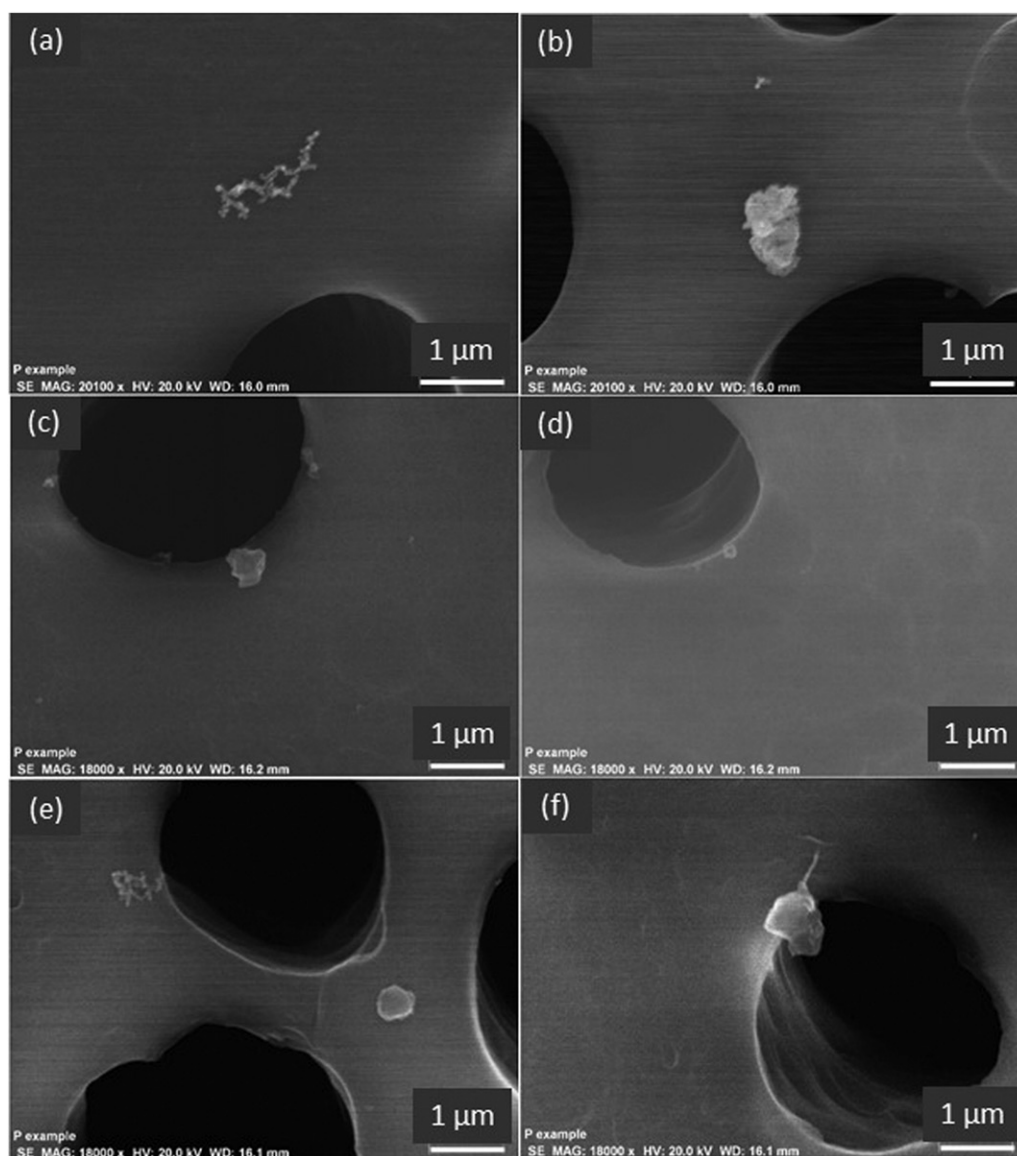


Figure 2. Morphology of exemplar particles emitted during operation of vat polymerization printers: (a) nanoscale-cluster particle observed in emissions from all printers; (b) aggregate particle emitted by the Form 1+ printer; (c) compact irregular particle emitted by the Pegasus Touch printer; (d) discrete spherical particle emitted by the Nobel 1.0A printer; (e) discrete spherical particle emitted by the Titan 1 printer; and (f) flake-like particle emitted by the M-One printer.

calculated using the printer-specific GM mobility diameters for particles emitted during printing. Among printers, deposition values were as follows: head region (3–7%), tracheobronchial region (9–21%), and pulmonary region (15–38%). Pulmonary deposition values for the DLP printers were about twice as great as the SLA printers. These estimates indicate potential for high numbers of particles containing various metals to deposit throughout the respiratory tract.

Total volatile organic compound emissions

Table 2 summarizes the calculated TVOC emission yield values during printing. Pairwise comparisons

revealed that the TVOC yield for the M-One was significantly higher than all other printers ($p < 0.05$) and the yield for the Titan 1 printer was significantly higher than for the Form1+, Pegasus Touch, and Nobel 1.0A printers ($p < 0.05$). The mean TVOC emission yield was significantly higher for DLP type printers compared to SLA printers ($p < 0.05$).

As summarized in Table S6, acetone, benzaldehyde, and 4-oxopentanal (4-OPA) were detectable during the printing and post-printing phases for specific combinations of printer and feedstock resin. There was no clear difference in carbonyl concentrations between types of printers. Acetone concentrations ranged from 0.7–18.0 ppb and from 0.9–26.0 ppb

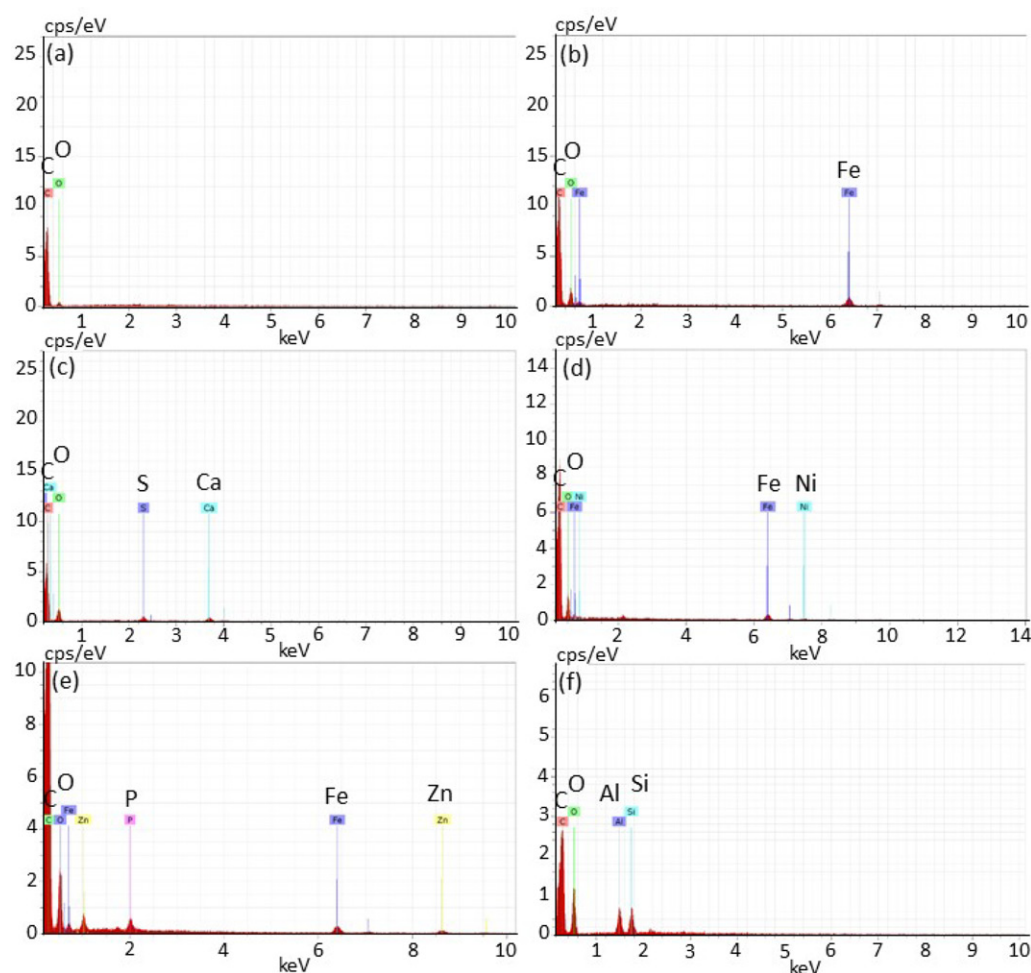


Figure 3. Elemental spectra illustrating the composition of exemplar particles emitted during operation of vat polymerization printers (spectra correspond to the particles shown in Figure 2): (a) representative carbon/oxygen particle observed in emissions from all printers; (b) iron-containing particle emitted by the Form 1+ printer; (c) calcium- and sulfur-containing particle emitted by the Pegasus Touch printer; (d) iron- and nickel-containing particle emitted by the Nobel 1.0A printer; (e) iron-, phosphorous- and zinc-containing particle emitted by the Titan 1 printer; and (f) aluminum- and silicon-containing particle emitted by the M-One printer.

Table 4. Regional lung deposition fractions for particles emitted by vat polymerization printers during operation.

Printer	Type	Head	Tracheobronchial	Pulmonary
Form 1+	SLA	0.0312	0.0926	0.1704
Pegasus Touch	SLA	0.0282	0.0866	0.1509
Nobel 1.0A	SLA	0.0330	0.0953	0.1804
Titan 1	DLP	0.0684	0.2115	0.3757
M-One	DLP	0.0383	0.1304	0.2744

during the print and post-printing phases, respectively. The highest acetone concentrations were observed from the Nobel 1.0A printer using XYZPrinting resin and were 18.1 and 26.0 ppb from the print and post-print sampling, respectively. Benzaldehyde concentrations ranged from 1.0–12.3 ppb and from 0.9–12.7 ppb during the print and post-printing phases, respectively. The highest benzaldehyde concentrations were observed from the M-One printer using Formlabs resin and were 12.3

and 12.7 ppb from the print and post-printing phases, respectively. 4-OPA concentrations were below the limit of detection, except for the Nobel 1.0A printer using XYZPrinting resin during post-print sampling, where a concentration of 0.07 ppb was observed.

Discussion

Results presented demonstrate that the vat polymerization printers emitted nanoscale and sub-micron scale particles and numerous organic vapors. The release of aerosol from the vat polymerization printers was insightful for understanding emissions because the build process consisted of hardening a bulk liquid resin using light rather than melting polymer (e.g., material extrusion) or spraying liquid droplets (e.g., material jetting) which are AM processes that are known to emit particles.^[1–7,9–11] Additionally,

differences in emissions were observed between the two types of printers: particle number, number of particles with sizes from 5.6–560 nm, and TVOC emission yields were significantly greater and GM particle sizes significantly smaller for DLP type printers compared to SLA printers ($p < 0.05$). The exact reason for this difference in emission yields between printer types is unclear at this time. It is unlikely that differences are related to the composition of the resins used in the SLA printers compared to DLP printers or from generation of heat by the exothermic hardening process because, as shown in Table 1, both the M-One DLP printer and the Form 1+ SLA printer were operated using the same gray resin (Formlabs). However, differences in light sources and principles of how resin is hardened offer a potential explanation. These SLA printers use a 405-nm wavelength laser to selectively harden discrete areas of resin, so only small discrete areas of the resin in the vat are exposed to the laser at any given moment. In contrast, the DLP printers use multi-wavelength light from a lamp in a projector to expose a larger area of resin as it projects the image onto the bottom of the vat and hardens the whole layer area at once. Hence, a potential explanation for the higher particle emission yields and smaller GM particle sizes from DLP printers may be an effect of a greater area of resin being cured at once (and possibly exposure of the resin to multiple wavelengths of light), which volatilizes resin constituents that condense in air to form particles. This explanation is supported by a recent report from Yang and Li who observed that build object surface area influences TVOC emissions (particle not measured in that study).^[12]

It is somewhat difficult to compare the yield data in Table 2 to existing reports in the literature for other types of AM processes because data from many studies are expressed in terms of ER values; however, this metric does not account for differences in amount of material processed among tests. Further complicating the inter-comparison of data is that different measurement methods and equations have been used among investigators to calculate ER and yield values for particles and chemicals.^[35] As such, standardized approaches to data collection and evaluation would be beneficial to allow inter-comparison of study results and strengthen the basis for conclusions regarding health and safety implications of AM processes.^[11] Supplemental File Table S7 summarizes emission yield data from available literature for common filaments used in desktop material extrusion printers as well as binder jetting, an AM process in which a liquid

bonding agent is selectively deposited to join powder materials. Results from the current evaluation of different types of vat polymerization printers indicated that particle emission yields were similar to material extrusion printers, i.e., about 1 to 9×10^8 #/g printed (P-Trak data) and 1 to 4×10^{10} # 5.6–560 nm/g printed (FMPS data) and at least 5 orders of magnitude higher than binder jetting printers.

It is known that a range of particle sizes are emitted during material extrusion, binder jetting, and powder bed fusion AM processes. Numerous investigators have reported particle size data for material extrusion, binder jetting, and powder bed fusion printers. The GM size of particles emitted during our chamber tests of the vat polymerization printers ranged from 15–45 nm, which is more similar to sizes released during material extrusion processes. The larger size of particles emitted during binder jetting and powder bed fusion AM processes may reflect the larger size of particles in the feedstock powder or droplets dispersed by nozzles used in those processes.

For all resins used in this study, the specific photoinitiator is proprietary or confidential on the respective Safety Data Sheets. As such, ICP analysis was used to identify elements in the bulk resins. Five elements were common to all resins (Al, Cr, P, Sn, and Ti), while Sb was present in two resins, and Ba, Cu, and Pb in one resin each (Supplemental Table S5). Of these elements, Al, Ba, Cu, Fe, Sb, and Ti are known photoinitiators.^[19–21,38] It is unclear if the other elements identified in the bulk resins by ICP or EDX analysis (Cr, P, Sn, and Pb) were intentionally included as photoinitiators, used to serve some other function, or are contamination from catalysts used for formulating oligomers. EDX analysis of airborne particles identified several elements that were quantified in the bulk resin (Al, Cr, P, and Ti) and printed objects (Al, Ca, Cr, Fe, Ni, P, Ti, and Zn) using ICP analysis. A detailed study of the mechanism of aerosol formation was beyond the scope of this study; however, we hypothesize that the presence of metals in the aerosol phase is from volatilization of resin constituents during curing, which subsequently condense in air to form particles. Mechanical disruption of the resin is unlikely because the vat moves only incrementally after each layer is formed. Bubble bursting is also unlikely because the resin temperature is maintained below its boiling point. Although not all elements quantified in the bulk resins or printed objects (e.g., Sb and Sn) were identified in the aerosol emissions, the commonality of several elements of health significance suggests that elemental analysis of feedstock

material and built objects provides insight to particle emissions chemistry. Future studies should focus on quantitative analysis of elements in emitted aerosol and understanding relationships with feedstock content as a means of screening for health risk of released aerosol. Concentrations of elements in the printed objects were generally higher than in the bulk feedstock resin, indicating an enrichment of materials during the printing process. Hence, consideration should be given for exposure potential to workers who manipulate these printed objects in a manner that generates dust (e.g., sanding, drilling). Interestingly, levels of Cd, Cr, Co, Ni, and V were higher in objects printed using the M-One DLP printer compared with the Form 1+ SLA printer, despite using the same resin (Supplemental Table S5). Additional research is needed to understand whether this observation is an effect of the type of printer technology or some other factor unknown to us at this time. Among the elements identified in the printed objects, Zn is known to be used as a photoinitiator.^[18] Overall, these data suggest that the chemistry of the resins, emissions, and printed objects is complex.

At this time, it is unclear why not all elements are present in these three matrices. As noted above, differences in elements identified among bulk resins could be from differences in manufacturer formulations or the presence of contaminants from catalysts used for formulating oligomers or other raw ingredients. Within a given resin, differences in elemental composition among the feedstock, released aerosol, and built object could be related to the initial amount of element, its form (metal, complex, etc.), and other factors such as density. In addition to these factors, there could be an influence of the analytical techniques employed in this study. As shown in Table 2, yield values for the FMPS were higher than for the P-Trak, indicating that a high proportion of particles had size less than 500 nm. The SEM images shown in Figure 2 illustrate that some particles had size above 500 nm. It is possible that the particle counting instruments are measuring the emissions (e.g., sub-500 nm range by FMPS) as they are released and these particles are captured with high efficiency on the filter. However, when we place the filter sample in the SEM, the vacuum and/or heat of the beam may be volatilizing the smallest/most volatile particles and only the larger particles with more mass remain visible in the microscope. Hence, the reported elemental composition of released particles may be incomplete if certain elements occur preferentially in smaller size particles. Recently, Gu et al.^[39] reported the potential for

smaller particle loss in the SEM because of particle volatility when monitoring aerosol released during material extrusion 3-D printing.

Results of human lung deposition modeling using GM particle sizes from the FMPS instrument indicate the potential for emitted particles to deposit in the head, tracheobronchial, and pulmonary regions of the respiratory tract (Table 4). Further evaluation of the temporal variation in size distribution data using the NanoPSDA software package revealed that the GM size of emitted particles was dynamic, i.e., initially decreased during printing and increased thereafter. These insights to the changing nature of the emitted size distributions suggest that regional particle lung deposition efficiency will vary over time with the age of the particles. For the examples presented in Figure 1, particle deposition in the alveolar region of the lung will increase as the size decreases, indicating that more particles will deposit if inhaled during the printing and post-printing phases compared to background. In both examples, the standard deviations of the GM particle sizes increased over the background, printing, and post-printing phases, reflecting the broader distribution of sizes (i.e., from 33–21 nm in Example B) as well as potential changes in the distribution from agglomeration or other particle interactions. Chemical analysis demonstrated that deposited particles would include multi-constituent particles composed of elements including Cr, Ni, Fe, and/or Zn. Deposition of particles such as welding fumes that contain Cr, Ni, and Fe in the head region has been shown to induce inflammation in the nasal passages.^[40] Deposition of particles containing these same elements throughout the head, tracheobronchial, and pulmonary regions of the respiratory tract can induce development of systemic inflammation.^[41] Inhalation of Cr and Ni also induces development of systemic immune sensitization.^[42] Additionally, many of these metals possess capacity to generate reactive oxygen species, which are implicated in various inflammatory and cellular alteration pathways in the lung.^[43] Toxicological evaluation of the vat printer emissions is needed to understand whether they present an inhalation risk for AM workers.

All vat polymerization printers emitted organic chemicals during printing. As summarized in Supplemental File Table S8, for volatile organic chemicals, yield values in published reports have been calculated using real-time photoionization detector measurements or off-line gas chromatography measurements for material extrusion printers. TVOC yield values calculated from our data for the SLA printers

(161–322 µg/g printed) were more similar to those reported for material extrusion printers whereas values for the DLP printers (1281–1931 µg/g printed) were higher. Yang and Li measured TVOC emissions with a photoionization detector during printing with a DLP-type vat polymerization printer.^[12] From the total mass of TVOC and print time reported by the authors, the estimated emission rates for their printer ranged from 8,000–26,000 µg/hr (object mass not reported, precluding calculation of yield). These values are consistent with our calculated emission rates of 14,300–18,500 µg/hr (Titan 1) and 20,000–23,700 µg/hr (M-One) for DLP-type machines.

The levels of three carbonyl compounds observed (acetone, benzaldehyde, and 4-OPA) from the printing and post-printing sampling phases exceeded the limits of detection and therefore could be measured. Although measurable, levels of acetone and benzaldehyde were well below their respective recognized occupational exposure limits of 250 ppm and 2 ppm (no limit available for 4-OPA).^[44,45] Since the concentrations for all three carbonyls were similar or greater during the post-printing process, this may indicate that their emissions could be the result of the resin curing process as the precursor chemicals are oxidized over time. This observed increase in concentrations suggests the potential for exposure to printer operators as well as among persons who handle objects after printing is completed. Other compounds could be emitted from these printing processes such as amines, carboxylic acids, or other oxygenated species. Hence, other analytical methods are needed to characterize the emissions more completely.

Conclusions

Despite using a bulk liquid resin feedstock, vat polymerization printers released particles and organic vapors during operation at levels that were similar to or exceeded those of other types of AM processes evaluated to date, including material extrusion which uses a heated nozzle to print. Mean particle and TVOC emission yields were significantly higher and GM particle sizes were significantly smaller for DLP type printers compared to SLA type printers, indicating an influence of printer technology on emissions. Particle deposition modeling indicates that emitted particles would deposit in the head region (3–7%), tracheobronchial region (9–21%), and pulmonary region (15–38%). Chemical analysis demonstrated that deposited particles would include multi-constituent particles composed of Cr, Ni, Fe, and/or Zn similar to

welding fume. Deposition of particles contain Cr, Ni, and Fe in the head region has been shown to induce inflammation in the nasal passages, systemic inflammation, systemic immune sensitization, and generate reactive oxygen species. Differences in emissions between SLA and DLP printers indicate that the underlying technology is an important factor when considering exposure reduction strategies such as engineering controls.

Acknowledgments

The authors wish to thank Kirk Scheckel at the U.S. EPA and Gary Roth at NIOSH for critical review of this manuscript before submission to the journal. The findings and conclusions in this article are those of the authors and do not necessarily represent the official position of the National Institute for Occupational Safety and Health, Centers for Disease Control and Prevention or the U.S. Environmental Protection Agency. Mention of any company or product does not constitute endorsement by the U.S. Government, National Institute for Occupational Safety and Health, Centers for Disease Control, or the U.S. Environmental Protection Agency.

ORCID

A. B. Stefaniak  <http://orcid.org/0000-0003-3914-1460>
T. P. Luxton  <http://orcid.org/0000-0003-1774-5407>
D. M. Peloquin  <http://orcid.org/0000-0002-4489-3475>

References

- [1] Azimi, P., D. Zhao, C. Pouzet, N.E. Crain, and B. Stephens: Emissions of ultrafine particles and volatile organic compounds from commercially available desktop three-dimensional printers with multiple filaments. *Environ. Sci. Technol.* 50:1260–1268 (2016).
- [2] Deng, Y., S.J. Cao, A. Chen, and Y. Guo: The impact of manufacturing parameters on submicron particle emissions from a desktop 3D printer in the perspective of emission reduction. *Build. Environ.* 104:311–319 (2016).
- [3] Floyd, E.L., J. Wang, and J.L. Regens: Fume emissions from a low-cost 3-D printer with various filaments. *J. Occup. Environ. Hyg.* 14:523–533 (2017).
- [4] Kim, Y., C. Yoon, S. Ham, et al.: Emissions of nanoparticles and gaseous material from 3D printer operation. *Environ. Sci. Technol.* 49:12044–12053 (2015).
- [5] Stabile, L., M. Scungio, G. Buonanno, F. Arpino, and G. Ficco: Airborne particle emission of a commercial 3D printer: The effect of filament material and printing temperature. *Indoor Air* 27:398–408 (2017).
- [6] Steinle, P.: Characterization of emissions from a desktop 3D printer and indoor air measurements in office settings. *J. Occup. Environ. Hyg.* 13:121–132 (2016).

- [7] **Stephens, B., P. Azimi, Z. El Orch, and T. Ramos:** Ultrafine particle emissions from desktop 3D printers. *Atmos. Environ.* 79:334–339 (2013).
- [8] **Yi, J., R.F. LeBouf, M.G. Duling, et al.:** Emission of particulate matter from a desktop three-dimensional (3-D) printer. *J. Toxicol. Environ. Health A* 79:453–465 (2016).
- [9] **Mendes, L., A. Kangas, K. Kukko, et al.:** Characterization of emissions from a desktop 3D printer. *J. Indust. Ecol.* 21:S94–S106 (2017).
- [10] **Vance, M.E., V. Pegues, S. Van Montfrans, W. Leng, and L.C. Marr:** Aerosol emissions from fuse-deposition modeling 3D printers in a chamber and in real indoor environments. *Environ. Sci. Technol.* 51:9516–9523 (2017).
- [11] **Zhang, Q., J.P.S. Wong, A.Y. Davis, M.S. Black, and R.J. Weber:** Characterization of particle emissions from consumer fused deposition modeling 3D printers. *Aerosol Sci. Technol.* 51:1275–1286 (2017).
- [12] **Yang, Y., and L. Li:** Total volatile organic compound emission evaluation and control for stereolithography additive manufacturing process. *J. Cleaner Prod.* 170:1268–1278 (2018).
- [13] **International Organization for Standardization:** Additive manufacturing — General principles — Terminology (ISO/ASTM 52900) [Standard]. Geneva, Switzerland, 2015.
- [14] **Short, D.B., D. Volk, P.D. Badger, J. Melzer, P. Salerno, and A. Sirinterlikci:** 3D printing (rapid prototyping) photopolymers: An emerging source of antimony to the environment. *3D Print. Addit. Manuf.* 1:24–33 (2014).
- [15] **Creytens, K., L. Gilissen, S. Huygens, and A. Goossens:** A new application for epoxy resins resulting in occupational allergic contact dermatitis: The three-dimensional printing industry. *Contact Dermatitis* 77:349–351 (2017).
- [16] **Fukumoto, I., A. Tamura, M. Matsumura, H. Miura, and N. Yui:** Sensitization potential of dental resins: 2-Hydroxyethyl methacrylate and its water-soluble oligomers have immunostimulatory effects. *PLoS ONE* 8:e82540 (2013).
- [17] **Heratizadeh, A., T. Werfel, S. Schubert, and J. Geier:** Contact sensitization in dental technicians with occupational contact dermatitis. Data of the Information Network of Departments of Dermatology (IVDK) 2001–2015. *Contact Dermatitis* (2018).
- [18] **Al Mousawi, A., C. Poriol, F. Dumur, et al.:** Zinc Tetraphenylporphyrin as high performance visible light photoinitiator of cationic photosensitive resins for LED projector 3D printing applications. *Macromolecules* 50:746–753 (2017).
- [19] **Czech, Z., A. Butwin, U. Gäuch, and J. Kabatc:** Influence of selected photoinitiators on important properties of photoreactive acrylic pressure-sensitive adhesives. *J. Appl. Polymer Sci* 123:118–123 (2012).
- [20] **Jakubiak, J., and J.F. Rabek:** Photoinitiators for visible light polymerization. *Polimery* 44:X1–461 (1999).
- [21] **Xiao, P., J. Zhang, D. Campolo, et al.:** Copper and iron complexes as visible-light-sensitive photoinitiators of polymerization. *J. Polymer Sci., Part A: Polymer Chem.* 53:2673–2684 (2015).
- [22] **House, R., N. Rajaram, and S.M. Tarlo:** Case report of asthma associated with 3D printing. *Occup. Med.* 67:652–654 (2017).
- [23] **Stefaniak, A.B., R.F. LeBouf, M.G. Duling, et al.:** Inhalation exposure to three-dimensional printer emissions stimulates acute hypertension and microvascular dysfunction. *Toxicol. Appl. Pharmacol.* 335:1–5 (2017).
- [24] **Chan, F.L., R. House, I. Kudla, J.C. Lipszyc, N. Rajaram, and S.M. Tarlo:** Health survey of employees regularly using 3D printers. *Occup. Med.* 68:211–214 (2018).
- [25] **Stefaniak, A.B., L.N. Bowers, A.K. Knepp, et al.:** Three-dimensional printing with nano-enabled filaments releases polymer particles containing carbon nanotubes into air. *Indoor Air* 28:840–851 (2018).
- [26] **ASTM:** 6670: Standard Practice for Full-Scale Chamber Determination of Volatile Organic Emissions from Indoor Materials/Products. West Conshohocken, PA, 2013.
- [27] **Moylan, S., J. Slotwinski, A. Cooke, K. Jurrens, and M.A. Donmez:** An additive manufacturing test artifact. *J. Res. Natl. Inst. Stand. Technol.* 119:429–459 (2014).
- [28] **Wells, J.R., and J.E. Ham:** A new agent for derivatizing carbonyl species used to investigate limonene ozonolysis. *Atmos. Environ.* 99:519–526 (2014).
- [29] **Bundesanstalt für Materialforschung und -prüfung (BAM):** Test Method for the Determination of Emissions from Hardcopy Devices RAL-UZ-205. [Standard] St. Augustin, Germany: BAM, 2017.
- [30] **Klein Entink, R.H., C. Bekker, W.F. Fransman, and D.H. Brouwer:** Analysis of time series of particle size distributions in nano exposure assessment. *J. Aerosol Sci.* 81:62–69 (2015).
- [31] **Klein Entink, R.:** NanoPSDA: Analysis of Time Series of Particle Size Distribution Data in Nano Exposure Assessment. R package version 1.0 ed, 2014.
- [32] **R-Code Team:** R: A Language and Environment for Statistical Computing. R package version 3.3.1 ed, 2016.
- [33] **Asgharian, B., W. Hofmann, and R. Bergmann:** Particle deposition in a multiple-path model of the human lung. *Aerosol Sci. Technol.* 34:332–339 (2001).
- [34] **ICRP:** International Commission on Radiological Protection. Publication 66: Human respiratory tract model for radiological protection Oxford, UK: Pergamon, 1994.
- [35] **Byrley, P., B.J. George, W.K. Boyes, and K. Rogers:** Particle emissions from fused deposition modeling 3D printers: Evaluation and meta-analysis. *Sci. Total Environ.* 655:395–407 (2019).
- [36] **Afshar-Mohajer, N., C.Y. Wu, T. Ladun, D.A. Rajon, and Y. Huang:** Characterization of particulate matters and total VOC emissions from a binder jetting 3D printer. *Build. Environ.* 93:293–301 (2015).
- [37] **Graff, P., B. Ståhlbom, E. Nordenberg, A. Graichen, P. Johansson, and H. Karlsson:** Evaluating measuring techniques for occupational exposure during additive manufacturing of metals: A pilot study. *J. Indust. Ecol.* 21:S120–S129 (2017).

- [38] **Short, D.B., A. Sirinterlikci, P. Badger, and B. Artieri:** Environmental, health, and safety issues in rapid prototyping. *Rapid Proto. J.* 21:105–110 (2015).
- [39] **Gu, J., M. Wensing, E. Uhde, and T. Salthammer:** Characterization of particulate and gaseous pollutants emitted during operation of a desktop 3D printer. *Environ. Int.* 123:476–485 (2019).
- [40] **Raulf, M., T. Weiss, A. Lotz, et al.:** Analysis of inflammatory markers and metals in nasal lavage fluid of welders. *J. Toxicol. Environ. Health A* 79:1144–1157 (2016).
- [41] **Kauppi, P., M. Jarvela, T. Tuomi, et al.:** Systemic inflammatory responses following welding inhalation challenge test. *Toxicol. Rep.* 2:357–364 (2015).
- [42] **Fireman, E., A.B. Shai, Y. Alcalay, N. Ophir, S. Kivity, and V. Stejskal:** Identification of metal sensitization in sarcoid-like metal-exposed patients by the MELISA(R) lymphocyte proliferation test — A pilot study. *J. Occup. Med. Toxicol.* 11:18 (2016).
- [43] **Leonard, S.S., G.K. Harris, and X. Shi:** Metal-induced oxidative stress and signal transduction. *Free Radic. Biol. Med.* 37:1921–1942 (2004).
- [44] **NIOSH:** "Pocket Guide to Chemical Hazards." Available at <http://www.cdc.gov/niosh/npg/default.html> (accessed March 15, 2019), 2010.
- [45] **Occupational Alliance for Risk Science:** "Workplace Environmental Exposure Levels." Available at <https://www.tera.org/OARS/WEEL.html> (accessed March 15, 2019), 2014.